Radiative impacts from biomass burning in the presence of clouds during boreal spring in southeast Asia

N. Christina Hsu

Goddard Earth Sciences and Technology Center, University of Maryland, Baltimore County, Baltimore, Maryland, USA

Jay R. Herman and Si-Chee Tsay

Laboratory for Atmospheres, NASA Goddard Space Flight Center, Greenbelt, Maryland, USA

Received 19 October 2002; revised 6 December 2002; accepted 21 January 2003; published 7 March 2003.

[1] The impact of smoke aerosols generated from biomass burning activities in Southeast Asia on the total (i.e., direct and indirect effects) reflected solar and emitted thermal radiation from clouds was investigated using satellite data. We combine narrowband radiance measurements, from ultraviolet to near-infrared wavelengths (e.g., SeaWiFS and TOMS), with broadband irradiance measurements (e.g., CERES) to quantify how smoke aerosols modulate the cloud radiative forcing. In Southeast Asia, our results reveal that smoke is frequently present over large areas of cloud-covered regions during boreal spring. The reflected solar (emitted thermal) radiation from clouds due to smoke aerosols can be reduced (enhanced) by as much as 100 (20) W m^{-2} over the month of March 2000. We also found that the reduction in cloud spectral reflectance at 670 nm is large enough to lead to significant errors in retrieving cloud properties (e.g., optical thickness and effective radius) from current satellite measurements, such as AVHRR and MODIS. *INDEX TERMS:* 0305 Atmospheric Composition and Structure: Aerosols and particles (0345, 4801); 0320 Atmospheric Composition and Structure: Cloud physics and chemistry; 0345 Atmospheric Composition and Structure: Pollution—urban and regional (0305); 0360 Atmospheric Composition and Structure: Transmission and scattering of radiation; 1610 Global Change: Atmosphere (0315, 0325); *KEYWORDS:* biomass burning, aerosols, clouds, radiative forcing, southeast Asia, monsoon. **Citation:** Hsu, N. C., J. R. Herman, and S.-C. Tsay, Radiative impacts from biomass burning in the presence of clouds during boreal spring in southeast Asia, *Geophys. Res. Lett.*, *30*(5), 1224, doi:10.1029/2002GL016485, 2003.

1. Introduction

[2] Over the last several years, increasing attention has been paid to the effects of tropospheric aerosols on Earth's overall radiation balance [*Penner et al.*, 1992; *Kaufman et al.*, 2002]. Most of this attention has been focused on understanding how aerosols modify the solar radiation budget over cloud-free scenes [*Hobbs et al.*, 1997; *Ross et al.*, 1998; *Haywood and Bougher*, 2000]. However, the effects of aerosols on radiative forcing due to clouds are even less well understood than over cloud-free scenes. Since cloud forcing is a much bigger component of the radiation budget, the effect of aerosols over clouds may have an even larger effect on radiative balance compared to aerosol forcing alone.

[3] Southeast Asia provides excellent atmospheric conditions to study such effects. Every boreal spring the indigenous populations of Laos, Thailand, Vietnam, Myanmar, and southern China clear the ground needed to plant agricultural crops by setting fires. While the fires are often set in areas that are relatively dry with little cloud cover (particularly in Myanmar, Thailand, and Laos), the smoke plumes they generate can stretch hundreds of kilometers into areas of heavy cloud cover (Vietnam and southern China). During the springtime, this cloud cover is generally composed of stratiform, low-altitude clouds associated with frontal systems that originate in China. Because both smoke and clouds converge over Vietnam and southern China, darkened (brown colored) clouds are often seen in satellite images during this season as smoke gets transported to areas that contain the low-lying cloud deck.

[4] In this paper, we combine data from three different satellite sensors (SeaWiFS, TOMS, and CERES) to examine how smoke aerosols generated from biomass burning activities in Southeast Asia affect the reflected solar and emitted thermal radiation from clouds contaminated with aerosol plumes.

2. Satellite Data Sets

[5] The SeaWiFS instrument was primarily designed to measure ocean color, and since its launch in 1997 it has been the major source for providing a comprehensive global data set of such measurements. However, the well-calibrated set of radiances measured in the wavelength range from the visible (0.41 μm) to the near infrared (NIR, 0.87 μm) is also well suited to providing true color imagery as well as information about atmospheric aerosols [*McClain et al.*, 1998]. There are two types of SeaWiFS data: 1 km resolution (LAC and HRPT) and 4 km resolution (GAC). In this analysis, we use the 4 km resolution Level-1 radiance data from SeaWiFS.

[6] Four different TOMS instruments have provided over 20 years of daily global measurements of UV radiances at six discrete wavelengths from 312 nm to 380 nm. The data set started in November 1978 and, with the exception of a data gap from January 1995 to August 1996, continues to the present day. While primarily designed to measure total column ozone amounts, TOMS UV measurements can also be used to study tropospheric aerosols through a quantity known as the aerosol index (AI) [*Hsu et al.*, 1996; *Herman*

0094-8276/03/2002GL016485$05.00

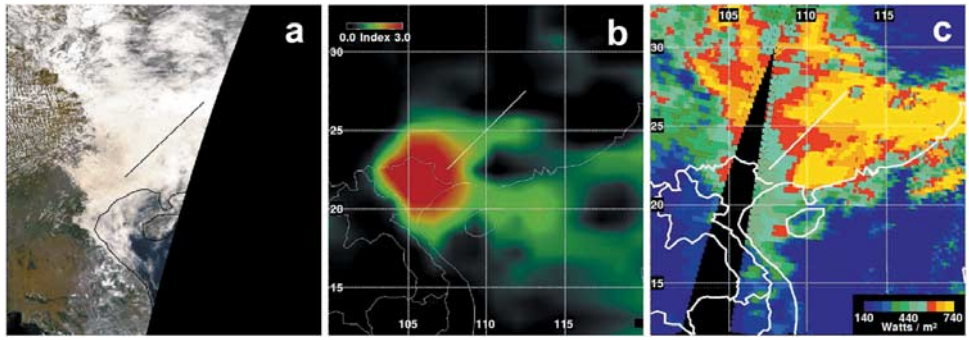

Figure 1. SeaWiFS true color image for Southeast Asia on 17 March 2000 is shown in (a), the corresponding TOMS AI in (b), and the CERES TOA upwelling shortwave flux in (c).

et al., 1997; *Torres et al.*, 1998]. Essentially, the AI is a measure of the wavelength-dependent change in Rayleigh scattered radiance from aerosol absorption relative to a pure Rayleigh atmosphere. The AI is defined in such a way that positive values generally correspond to UV-absorbing aerosols and negative values to non-absorbing aerosols. In this study, we use AI data from Earth Probe (EP) TOMS (1996 to present). The footprint size for EP TOMS is roughly 40 × 40 km^2 at nadir. The TOMS AI data are especially suitable for detecting the presence of absorbing aerosols over high reflecting surfaces, such as clouds and snow/ice [*Hsu et al.*, 1999]. Model simulations have shown that the TOMS AI can distinguish between a thin cloud and absorbing aerosols (Z. Ahmad et al., Properties of backscattered ultraviolet reflectances in cloudy atmosphere, submitted to *Journal of Geophysical Research,* 2002).

[7] The CERES sensor is an advanced version of the ERBE instrument and provides radiometric measurements of the Earth-atmosphere system from three broadband channels. In this analysis we use CERES data from the Terra satellite, launched in December 1999. The primary products include shortwave (0.3–5 μm), longwave (5–200 μm), and total (0.3–200 μm) radiation flux [*Wielicki et al.*, 1996]. An angular distribution model (ADM) is required to convert observed radiances to the flux products mentioned above. The shortwave flux error due to the ADM is estimated to be a 1.0% bias with a standard deviation of 12%, while the longwave flux error is estimated to be a 0.5% bias with a standard deviation of 5% [*Suttles et al.*, 1992; *Wielicki et al.*, 1996]. In order to obtain radiation measurements with the smallest footprint, we focus on the CERES ES-8 scanner data, with footprint size of approximately 20 × 20 km^2 at nadir.

3. Example of Smoke-Cloud Conditions in Southeast Asia

[8] To study an example of conditions typically seen over this area in the spring, we investigated the effect of smoke on 17 March 2000. On this day, several large smoke plumes generated from biomass burning were observed in cloud-free skies over Laos, Thailand, and Myanmar. The prevailing wind in this region is, in general, westerly for this time of the year, and the smoke was carried to the east. The SeaWiFS true color image for this day, depicted in Figure 1a, clearly shows smoke that has drifted eastward into a cloudy area located in northern Vietnam to southern China and darkened a significant portion of it.

[9] The collocated TOMS AI spatial distribution (cf. Figure 1b) shows enhanced aerosol index values (AI > 4) in the region where smoke is seen in the same area as the cloudbank. However, the haze layer over Laos, Thailand, and Myanmar under cloud-free conditions does not have as high an AI signal, probably because of reduced sensitivity of TOMS AI to absorbing aerosols that are low in the atmosphere and close to the low-reflecting surface. Correspondingly, the CERES TOA upwelling shortwave (SW) flux for the same region is shown in Figure 1c. It is apparent that for overcast conditions the CERES SW flux (Figure 1c) shows a high negative correlation with the TOMS AI (Figure 1b) and the reduced cloud reflectivity in the SeaWiFS true color image (Figure 1a). To further investigate the consequence of smoke impact on clouds, a transect line that crosses from the smoke-free clouds to the smoke-laden clouds has been drawn as target area.

4. Analysis of Spectral Signature

[10] To examine how the presence of such smoke aerosols changes the overall cloud spectral reflectivity, we calculate the Lambertian equivalent reflectivity for a given wavelength λ, R_λ (*cf. Herman and Celarier* [1997] for the heritage), derived using the SeaWiFS Level-1 radiances from the 412nm (blue), 670nm (red), and 865nm (NIR) channels for this region.

[11] The values of R_{412}, R_{670}, and R_{865} are shown in Figure 2 (upper panel) as a function of longitude along the transect line (cf. Figure 1). The cloud reflectivity from all three channels is seen to decrease from the white-cloud regime in the eastern part of the transect line (longitude >111°E) to the smoke-laden cloud regime in the western part (longitude <111°E). While smoke aerosols scatter and absorb solar radiation at the same time, the effect of absorption is further enhanced over scattering when smoke layers are over a high reflecting surface, due to multiple reflection between the atmosphere and the surface. It results in a higher probability for photons to be absorbed by smoke aerosols and thus less photons escape to space. The reflectivity decreases shown in Figure 2 are approximately 10% (from 90% to 80%) for the 865 nm channel, 20% (from 86% to 70%) for the 670 nm channel, and 30% (from 86% to 60%) for the 412 nm channel. As a result, the spectral

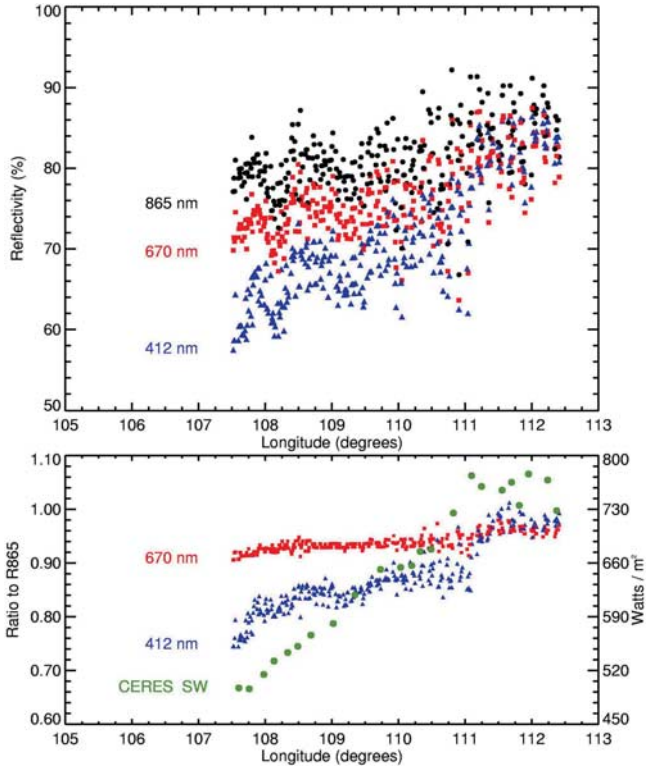

Figure 2. (Upper panel) Reflectivity for 865 nm (black), 670 nm (red), and 412 nm (blue) along the transect line from smoke-free clouds to smoke-laden clouds as shown in Figure 1. (Bottom panel) The ratios of the 670 nm and 412 nm reflectivities to the 865 nm reflectivity. The variability in the ratio of reflectivity values between two channels is much smaller than reflectivity from each individual channel, due to the suppression of the angular effect. The CERES shortwave flux is superimposed with the scale showing on the right Y-axis.

dependence of the cloud reflectivity is different over smoke-laden clouds when compared to the much smaller spectral dependence over smoke-free clouds. The 670 nm is the sole channel for retrieving optical thickness, and since the reduction in cloud reflectance due to absorbing aerosols is not accounted for in the current cloud algorithms, this effect will cause significant errors in the retrieved cloud properties (such as cloud optical thickness and effective radius).

[12] Figure 2 (bottom panel) indicates that the percentage reduction in radiation over smoke-laden clouds is the largest in blue light compared to longer wavelengths. These large reductions in the shorter wavelength compared to longer wavelength are not only due to the larger optical thickness of the smoke layer at the shorter wavelength. The molecular scattering optical thickness increases drastically as the wavelength becomes shorter, and this enhances the probability for photons to be absorbed by smoke layers. Superimposed in this figure are the corresponding CERES SW fluxes (denoted by green filled circles) on a single pixel resolution along the same transect line. The values of these SW fluxes were seen to decrease significantly from white clouds to smoke-laden clouds, while the values of the TOMS AI (cf. Figure 1b) increase from near zero to about 3.

5. Statistical Analysis of Aerosol Effect on Cloud Forcing

[13] In order to investigate the seasonal radiative impact of smoke on clouds in this region, we generated a collocated data set by averaging the daily Level-2 data from all three sensors into 0.5° latitude by 0.5° longitude bins for the entire month of March 2000. We then combined SW and total (SW + LW) flux from CERES with AI from TOMS and reflectivity from SeaWiFS for each grid box within the region bounded by the latitudes 15°N–30°N and the longitudes 100°E–125°E. To prevent sub-pixel (broken) cloud contamination, we adopt a criterion that the reflectivity derived from the SeaWiFS 865 nm channel, R_{865}, has to be greater than 70%. Two types of histograms were generated from this data set; one for relatively smoke-free clouds (AI < 0.1, non-shaded) and one for smoke-laden clouds (AI >1.5, shaded). The results for SW flux and total (SW + LW) flux are depicted in Figures 3a and 3b, respectively. The solar zenith angles for the region of interest are approximately 20°–30°.

[14] For the case of relatively smoke-free clouds, Figure 3a illustrates that the TOA upwelling SW flux peaks at 720–740 W m^{-2} for this region during March. In contrast, when smoke is observed to be in the cloudy areas of the same geographic region, the resulting peak of the TOA SW flux during the same season is reduced to about 620–640

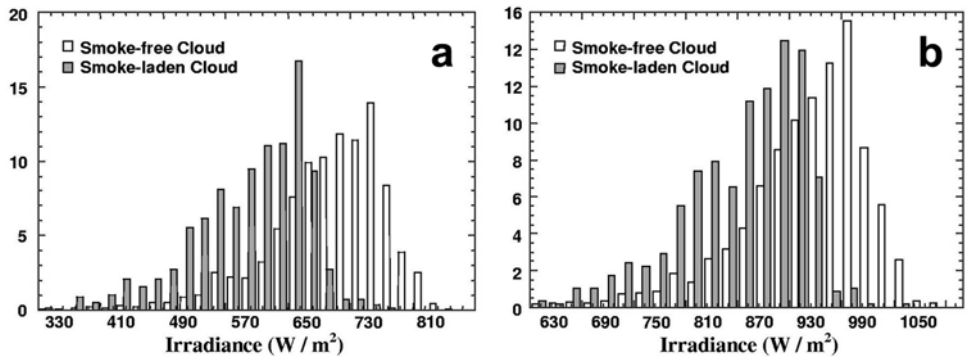

Figure 3. The monthly histograms of the TOA upwelling (a) shortwave, and (b) total (shortwave + longwave) flux for the region of 15°–30°N and 100° –125°E during March 2000 over smoke-free clouds (non-shaded), and over smoke-laden clouds (shaded). All of the histograms have been normalized to 100.

Wm^{-2}. Therefore, the reduction in outgoing SW flux when smoke aerosols occur in cloudy regions is substantial. This would in turn cause a strong warming in the smoke layer above the cloud deck.

[15] The corresponding TOA upwelling total flux peaks at about 960–980 W m^{-2} over smoke-free clouds for this region during March, while the total flux over smoke-laden clouds peaks at 880–920 W m^{-2}. The reduction in the total flux due to the presence of the smoke aerosol is around 70–80 W m^{-2}. This is because the LW flux increases by about 20–30 W m^{-2} over the smoke-laden clouds when compared to that over smoke-free clouds, and thus compensates for some of the reduction in the SW flux, resulting in a slightly smaller net reduction in the total flux. An enhancement of the temperature inversion by SW absorption may be one of the processes that leads to an increase in LW emission when smoke aerosols are in cloudy areas. To fully understand the processes it requires more *in situ* measurements of the radiation fields and temperature profiles over the cloud top along the transect line.

6. Concluding Remarks

[16] In this study, we demonstrated that large differences in the reflected solar and emitted thermal radiation from clouds occur when smoke aerosols are transported over and interact with clouds. The differences in shortwave flux can be 100 W m^{-2} or more, which is a significant component of the total radiative budget. Since this observed difference may be a combination of direct effects (absorption of sunlight above the cloud) and indirect effects (mixing and interacting with low clouds), more ground-based and aircraft measurements are urgently needed to fully understand and partition the contributions from both.

[17] Furthermore, such large perturbations in radiation fields (SW + LW) will induce an imbalance in the terrestrial heat budget that could affect local wind circulation patterns and cloud dynamics. This, in turn, may lead to drastic change when the Southeast Asian monsoon begins, currently in the late boreal spring and early summer. Perturbations in the onset of the Southeast Asian monsoon are believed to have great influence on the development of full-scale Asian summer monsoons during the subsequent months [*Lau and Yang*, 1997]. Therefore, better quantification of the smoke effect on clouds in the radiative budget is crucial to the improvement of the predictability of the tropical climate system during the boreal spring.

[18] **Acknowledgments.** We would like to thank the SeaWiFS processing team for providing well calibrated radiance data and the NASA Langley Distributed Active Archive Center (DAAC) for providing the CERES data. We would also like to thank the reviewers for their constructive comments.

References

Haywood, J., and O. Bougher, Estimates of the direct and indirect radiative forcing due to tropospheric aerosols: A review, *Rev. Geophys.*, *38*, 513–543, 2000.

Herman, J. R., and E. A. Celarier, Earth surface reflectivity climatology at 340–380 nm from TOMS data, *J. Geophys. Res.*, *102*, 28,003–28,011, 1997.

Herman, J. R., P. K. Bhartia, O. Torres, C. Hsu, C. Seftor, and E. Celarier, Global Distribution of UV-absorbing aerosols from Nimbus-7/TOMS data, *J.Geophys. Res.*, *102*, 16,911–16,922, 1997.

Hobbs, P. V., J. S. Reid, R. A. Kotchenruther, R. J. Ferek, and R. Weiss, Direct radiative forcing by smoke from biomass burning, *Science*, *275*, 1776–1778, 1997.

Hsu, N. C., J. R. Herman, P. K. Bhartia, C. J. Seftor, O. Torres, A. M. Thompson, J. F. Gleason, T. F. Eck, and B. N. Holben, Detection of biomass burning smoke from TOMS measurements, *Geophys. Res. Lett.*, *23*, 745–748, 1996.

Hsu, N. C., J. R. Herman, J. F. Gleason, O. Torres, and C. J. Seftor, Satellite detection of smoke aerosols over a snow/ice surface by TOMS, *Geophys. Res. Lett.*, *26*, 1165–1168, 1999.

Kaufman, Y. J., D. Tanre, and O. Boucher, A satellite view of aerosols in the climate system, *Nature*, *419*, 215–223, 2002.

Lau, K.-M., and S. Yang, Climatology and interannual variability of the southeast Asian summer monsoon, *Adv. Atmos. Sci.*, *14*, 141–162, 1997.

McClain, C. R., M. L. Cleave, G. C. Feldman, W. W. Gregg, S. B. Hooker, and N. Kuring, Science quality SeaWiFS data for global biospheric research, *Sea Technol.*, *39*, 10–16, 1998.

Penner, J. E., R. E. Dickinson, and C. A. O'Neill, Effects of aerosol from biomass burning on the global radiation budget, *Science*, *256*, 1432–1433, 1992.

Ross, J. L., P. V. Hobbs, and B. Holben, Radiative characteristics of regional hazes dominated by smoke from biomass burning in Brazil: Closure tests and direct radiative forcing, *J. Geophys. Res.*, *103*, 31,925–31,941, 1998.

Suttles, J. T., B. A. Wielicki, and S. Vemury, Top-of-atmosphere radiative fluxes-Validation of ERBE scanner inversion algorithm using Nimbus-7 ERB data, *J. Appl. Meteorol.*, *31*, 784–796, 1992.

Torres, O., P. K. Bhartia, J. R. Herman, Z. Ahmad, and J. Gleason, Derivation of aerosol properties from satellite measurements of backscattered ultraviolet radiation: Theoretical basis, *J. Geophys. Res.*, *103*, 17,099–17,110, 1998.

Wielicki, B. A., B. R. Barkstrom, E. F. Harrison, R. B. Lee III, G. L. Smith, and J. E. Cooper, Clouds and the Earth's Radiant Energy System (CERES): An Earth Observing System Experiment, *Bull. Am. Meteorol. Soc.*, *77*, 853–868, 1996.

N. C. Hsu, GEST, University of Maryland, Baltimore County, 1000 Hilltop Circle, Baltimore, MD 21250, USA. (hsu@wrabbit.gsfc.nasa.gov)

J. R. Herman and S. C. Tsay, NASA Goddard Space Flight Center, Code 916, Greenbelt, MD 20771, USA. (herman@tparty.gsfc.nasa.gov; tsay@climate.gsfc.nasa.gov)